Resource limitation modulates the fate of dissimilated nitrogen in a dual-pathway Actinobacterium

David C. Vuono[a], Robert W. Read[a], James Hemp[b], Benjamin W. Sullivan[c], John A. Arnone III[a], Iva Neveux[a], Bob Blank[d], Carl Staub[e], Evan Loney[a], David Miceli[a], Mari Winkler[f], Romy Chakraborty[g], David A. Stahl[f], Joseph J. Grzymski[a,*]

[a]Division of Earth and Ecosystem Sciences, Desert Research Institute, Reno, NV 89512, USA

[b]Division of Geological and Planetary Sciences, California Institute of Technology, Pasadena, CA, USA

[c]Department of Natural Resources and Environmental Science, University of Nevada, Reno, NV 89557, USA

[d]Agricultural Research Service, U.S. Department of Agriculture, Reno, NV, 89512, USA

[e]Agtron, Inc. 9395 Double R Blvd, Reno, NV 89521, USA

[f]Department of Civil and Environmental Engineering, University of Washington, Seattle, WA, 98195, USA

[g]Lawrence Berkeley National Laboratory, Berkeley, CA, 94729, USA

[*]Correspondence: Joseph J. Grzymski, Division of Earth and Ecosystem Sciences, Desert Research Institute, Reno, 2215 Raggio Parkway, NV 89512, USA

Email: Joe.Grzymski@dri.edu

Abstract

Respiratory ammonification and denitrification are two evolutionarily unrelated dissimilatory nitrogen (N) processes central to the global N cycle, the activity of which is thought to be controlled by carbon (C) to nitrate (NO_3^-) ratio. Here, we find that *Intrasporangium calvum* C5, a novel menaquinone-based dual-pathway denitrifier/respiratory ammonifier, disproportionately utilizes ammonification rather than denitrification when grown under carbon or nitrate limitation, not C:NO_3^- ratio. Higher growth rates are promoted by ammonification and metabolite and transcriptional profiles during growth show that the bacterium produces its own formate from a fermentable carbon source (lactate) to further generate a proton motive force for the ammonification pathway. Transcript abundances encoding for nitrite reducing enzymes, NrfAH and NirK, also significantly increase in response to nitrite production. Mechanistically, our results suggest that pathway selection is driven by intracellular redox potential (redox poise), which is lowered during resource limitation, thereby decreasing catalytic activity of upstream electron transport steps needed for denitrification enzymes. Our work advances our understanding of the biogeochemical tapestry of N-cycle dynamics and pathway evolution.

Globally, respiratory ammonification and denitrification are vital nitrogen (N) dissimilation pathways that either retain reactive N to support net primary productivity or close the N-cycle through the release of gaseous N, respectively[1]. The environmental controls on these two pathways, particularly the ratio of electron-donor to electron-acceptor (e.g., C:NO_3^-)[2], have gained attention[3–7] due to increased anthropogenic N inputs into the environment[8]. However, the effects of resource limitation on growth and pathway selection (i.e., allocation of C and N to dissimilatory and assimilatory processes), which are often confounded by C:NO_3^- ratio, have not been tested. Strong selective pressures from Earth's shifting biogeochemistry and oxidation-state have driven evolutionary adaptions to microbial electron transport chains (ETC)[9,10], respiratory chain redox potentials[11–13], and protein atomic composition[14,15], may shed light on how these pathways are regulated in contemporary organisms. Here, by identifying the biochemical and evolutionary differences between respiratory ammonification and denitrification, we disentangle the functional significance and molecular mechanisms of electron transfer through either pathway in a dual pathway organism.

48 From a biochemical standpoint, the primary difference between respiratory ammonification and
49 denitrification is their respective source of reducing equivalents in the ETC: 1) heme-based
50 cytochrome c nitrite reductase used in respiratory ammonification receive electrons directly from
51 the quinone (Q) pool[16] while 2) copper and cd_1 nitrite reductases used in denitrification receive
52 electrons from a soluble electron carrier (e.g., cytochrome c) via the bc_1 complex[17]. From an
53 evolutionary standpoint, we can place each N-module's origin to a putative time in Earth history
54 based on the metal co-factors that would have been bioavailable: heme-based cytochromes in an
55 ancient, more reduced, environment compared to the copper-containing nitrite reductases in an
56 oxidizing environment[18]. The bioenergetic chains of microorganisms also underwent selective
57 pressure to shift from low-potential (LP) to high-potential (HP) quinones in response to Earth's
58 oxygenation[11,12]. Menaquinone (MK) is thought to be the ancestral type of LP quinone[19].
59 Organisms that use ubiquinone (UQ) are thought to have evolved under high O_2 tensions with α-,
60 β-, γ-proteobacteria as the only bacterial clades to use UQ[12]. Surprisingly, our understanding for
61 the biochemistry of denitrification is based predominantly on HP UQ-based systems[20], leaving a
62 significant knowledge gap in the physiology and biochemistry of LP MK-based denitrifiers and
63 how they link electron transfer with energy capture under resource limitation[21–23].

64 As a predicted environmental control for respiratory ammonification versus denitrification,
65 $C:NO_3^-$ ratio, the predicted end-products should remain identical at different substrate
66 concentrations of the same ratio. In order to resolve the mechanisms of $C:NO_3^-$ control on
67 pathway selection and better understand branched respiratory chains in LP-based nitrate-
68 reducing organisms, we undertook the characterization of the novel Gram-positive
69 Actinobacterium strain *Intrasporangium calvum* C5: a dual-pathway nitrite reducer that uses MK
70 as sole pool quinone. Here we show that over a range of $C:NO_3^-$ ratios, duplicated at two
71 substrate concentrations, *I. calvum* disproportionately utilizes its ammonia-forming pathway
72 during C limitation ($\leq$ 0.4mM lactate), when $C:NO_3^-$ ratios are < 1 (an observation contrary to the
73 current paradigm). Using a genome-guided approach coupled to time-series transcriptomics and
74 metabolite profiles, we identified differentially expressed genes in the bacterium's ETC and
75 central metabolic pathways. Using this information to inform a metabolic reconstruction of the
76 ETC we infer mechanisms by which these two pathways are regulated at the biochemical level.

77 **Results**

78 **Genomic analysis of *I. calvum* C5.** We sequenced and analyzed the genome of *I. calvum* C5 to
79 first compare its similarity to the type species *I. calvum* 7KIP. We identified a high degree of
80 sequence similarity to 7KIP based on three homologous sequence regions as locally collinear
81 blocks (SI Results). Genome size of C5 was 4,025,044 base pairs (bp), only 662 bp longer than
82 7KIP. Genomic analysis of the ETC revealed the typical suite of complexes common to
83 facultative aerobes, including primary dehydrogenases (*nuo* complex, succinate dehydrogenase),
84 alternative *NDH-2* NADH dehydrogenase, cytochrome bc_1 complex, high-oxygen adapted
85 cytochrome c oxidase (A-family), and low-oxygen adapted cytochrome *bd* oxidase. The bc_1
86 complex subunits are also located immediately upstream of cytochrome c oxidase, suggesting
87 that these enzymes are encoded in a single operon creating a supercomplex. Despite *I. calvum*'s
88 seeming propensity for aerobic growth on a number of growth media[24], its bioenergetic system
89 uses MK as its sole pool quinone. *I. calvum* also possesses multiple pathways for supplying
90 electrons into the MK-pool, such as formate, malate, hydroxybutyrate, and glycerophosphate
91 dehydrogenases. Once in the MK-pool, there are alternative pathways for MKH_2 oxidation that
92 can circumvent the bc_1 complex, such as a membrane-bound respiratory nitrate reductase module
93 (NarG). In addition, to NarG, its dissimilatory N module composition consists of a truncated
94 denitrification pathway (N_2O is a terminal product) using a copper nitrite reductase NirK and
95 quinol-dependent nitric oxide reductase qNor. *I. calvum* also possesses both catalytic and
96 membrane anchor subunits (NrfA and NrfH, respectively) for a pentaheme cytochrome c module
97 involved in respiratory nitrite ammonification.

98 ***I. calvum* encodes for a functional NrfAH complex and assimilates NH_4^+ via respiratory**
99 **nitrite ammonification.** To gain insight into possible function of the NrfAH complex, we
100 aligned the NrfA protein sequences from C5 and 7KIP to a collection of 33 recognized
101 cytochrome c nitrite reductases from published annotated genomes (Table *S1*). This confirmed
102 that NrfA from *I. calvum* is a member of the CxxCH 1st heme motif group (Figure *1*A), which
103 forms one of four clades on the NrfA phylogenetic tree. We then queried the genomes of the taxa
104 in our phylogeny for other annotated N-reducing modules used in nitrate reduction, nitrite
105 reduction, NO-forming nitrite reduction, and primary pool quinone. Among the three major
106 clades of NrfA, at least 5 additional taxa are noted having dissimilatory N-module inventories
107 containing dual respiratory pathways: *S. thermophilum, B. azotoformans, B. bataviensis*, *B.*
108 *bacteriovorus*, and *Candidatus* N. inopinata, (Figure *1*A). None of the taxa in

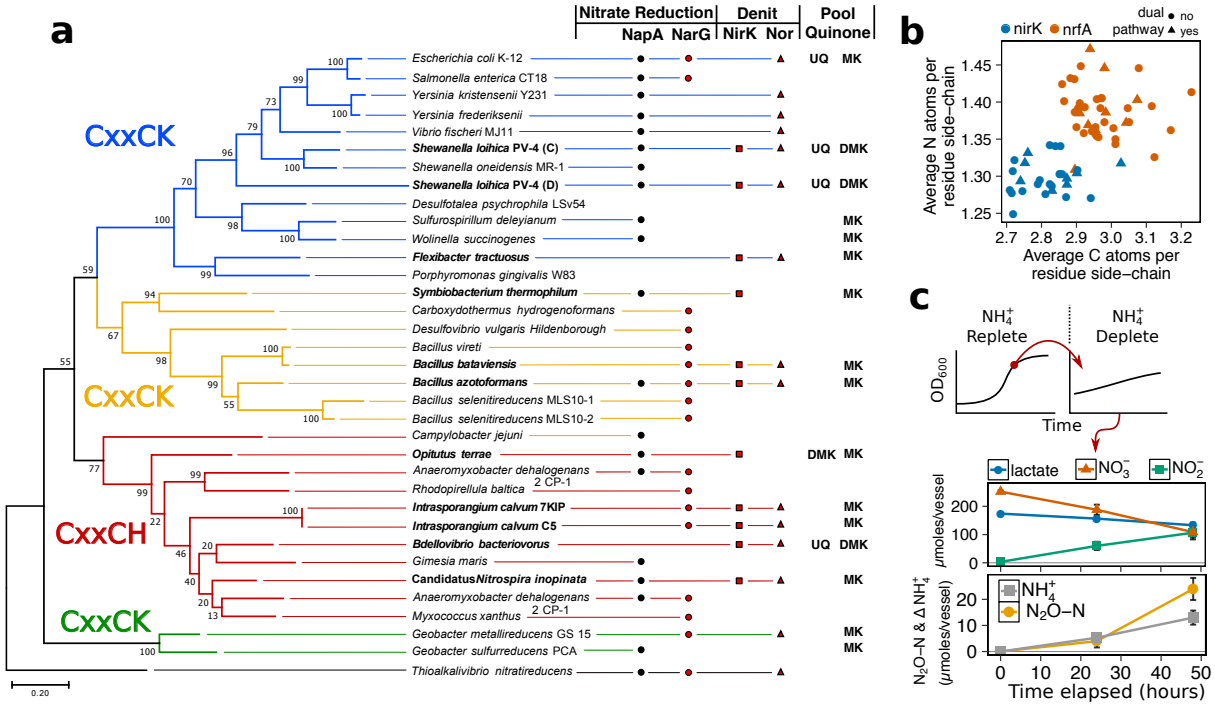

Figure 1. (A) Maximum likelihood phylogenetic tree of NrfA amino acid sequences from known respiratory ammonifiers and accompanying N-module composition for each organism. Pool quinone is also noted for dual-pathway nitrite reducers and model species. Colors of the main branches denote the 1st heme motif type: CxxCK and CxxCH. (B) Protein atomic composition for N and C normalized to protein length for NirK and NrfA nitrite reductases. (C) State-transition from ammonium-replete to ammonium-deplete for I. calvum C5 grown under 8mM lactate 12mM nitrate minimal media at 30 ºC. Metabolite profiles for ammonium-deplete are shown.

our NrfA phylogeny harbored the cd_1 nitrite reductases (NirS). Due to the exclusive NirK representation in dual-pathway membership, we asked whether there might be differences in protein atomic composition between NirK and NrfA, given the disparate evolutionary origins of these modules[25]. We collected 20 additional publicly available NirK protein sequences from nondual-pathway denitrifiers (Table *S1*) and calculated the protein C and N composition for our NirK/NrfA collection as atoms per residue side-chain (Figure *1*B). These results showed a significant depletion in C and N per residue side-chain for NirK compared to NrfA (C and N: $p<0.001$; t-test), indicating that resource constraints are imprinted on the evolution of these proteins.

We next tested the functionality of *I. calvum*'s Nrf complex by growing the bacterium under reducing conditions (8 mM lactate, 12 mM nitrate, ammonium-replete). We then performed a state-transition where biomass from late-exponential growth phase was collected and

130 anaerobically inoculated into ammonia-deplete media (Figure *1*C; SI Results). Despite no
131 detectable amounts of ammonium produced in the media over time, cell counts increased
132 $5.4x10^5 \pm 8.9x10^4$ cells/mL (0.126±0.02 optical absorbance units, OD_{600}) over a 48-hour
133 incubation, indicating consumption of ammonium produced by NrfA. Net ammonium production
134 was 13±2.7 µmoles with the remainder of dissimilated N being used by the denitrification
135 pathway (24±4.2 µmoles N_2O-N), resulting in a recovery of 97.4% dissimilated N. These results
136 confirmed that *I. calvum* C5 has a functional Nrf complex and also consumes the product
137 (ammonium) of respiratory nitrite ammonification.

138 **Respiratory nitrite ammonification exceeds denitrification under C-limitation.** We
139 investigated C:NO_3^- control on respiratory ammonification versus denitrification on cultures of *I.*
140 *calvum* C5 over a high resource C:NO_3^- range (16-0.4 mM lactate, 12 mM nitrate; ratio 4-0.1)
141 and low resource C:NO_3^- range (1.6-0.04 mM lactate, 1.2 mM nitrate; ratio 4-0.1). This
142 experimental design enabled us to evaluate C:NO_3^- control over a broader range than previous
143 studies that only considered ratios ≥ 1.5[3,4,26], while also testing the effects of resource
144 concentration on pathway selection. Under all the treatments tested, gas and ion chromatography
145 measurements showed products of both respiratory pathways, differing only in the relative
146 fraction of N_2O versus ammonium production across treatments (Figure *2*). At high resource
147 concentrations, respiratory ammonification did not prevail at high C:NO_3^- ratios (Figure *2*A,
148 Figure *2*B, left panels; Table *S2*). Instead, significantly greater amounts of N_2O were produced
149 over ammonium, though nitrite was still the major extracellular end-product of nitrate
150 respiration. Despite the predominance of N_2O production under the high resource concentrations,
151 ammonium production exceeded N_2O production only at the lowest C:NO_3^- ratio (0.4 mM
152 lactate, ratio=0.1) (Figure *2*) and accounted for 76.2±0.1% of dissimilated N.

153 Results from the low resource dataset provided weak support for the strict stoichiometry
154 hypothesis that C:NO_3^- controls pathway selection. Ammonia exceeded N_2O production only
155 under one high C:NO_3^- ratio treatment (ratio=4; 1.6 mM lactate; Figure *2*A, Figure *2*B, right
156 panels). However, at ratios ≤1 (≤0.4 mM lactate), significantly more ammonium than N_2O was
157 produced. On average, respiratory ammonification accounted for 78.1±8.9% of dissimilated N
158 for lactate concentrations ≤0.4 mM. When these results are taken in context with cell physiology,
159 we observed a significant and positive relationship between specific growth rate (μ) and the

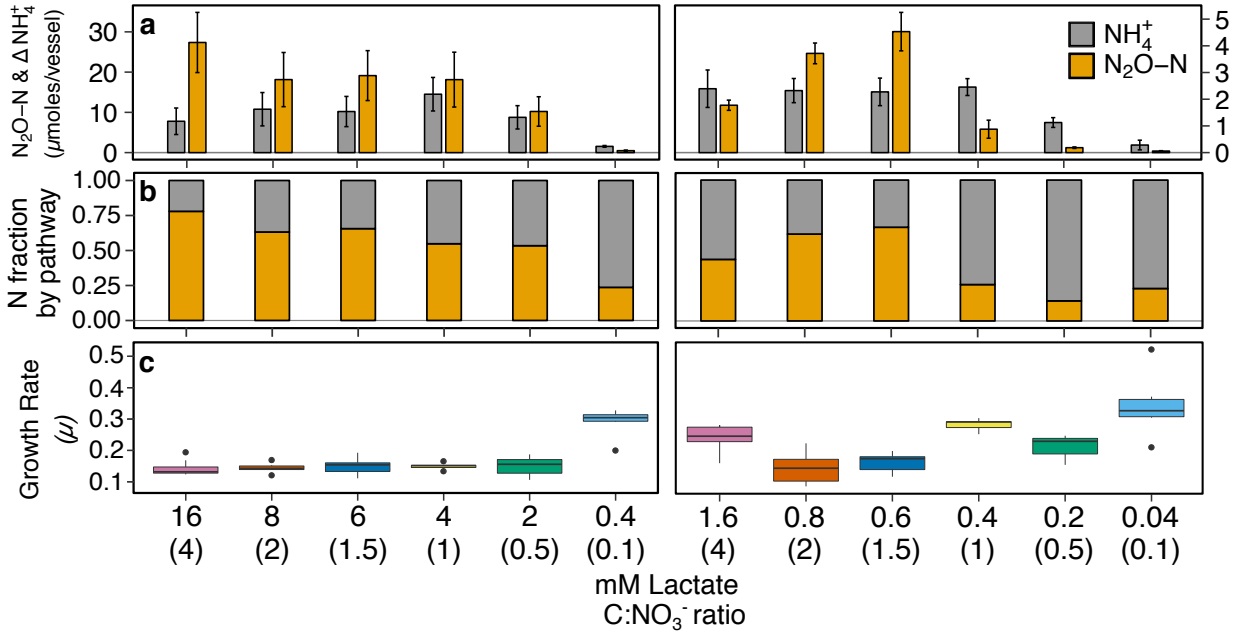

Figure 2. The effects of high resource (left; range of lactate concentrations with 12 mM NO_3^-) and low resource (right; range of lactate concentrations with 1.2 mM NO_3^-) concentrations with the same C:NO_3^- ratio on pathway selection in I. calvum C5. (A) Production of N_2O-N and net change of NH_4^+ over a 100-hour incubation period at 30 ºC. Each bar represents the average of 8-10 replicates per treatment (Table S5). (B) Fraction of dissimilated N by pathway. (C) Growth rates for each corresponding treatment. The x-axis label defines lactate concentration and C:NO_3^- ratio in parentheses.

fraction of N dissimilated by respiratory ammonification (R^2=0.5; p<0.001) (Figure *2*C, S1; Table S3).

Resource concentration influences the metabolite profiles of ammonium and N_2O production. Given the co-occurrence of end products from both pathways during the end-point experiments (Figure *2*), we next investigated the timing of ammonium and N_2O production relative to metabolite profiles for lactate, nitrate/nitrite, and growth phase at two resource concentrations with the same ratio (8 mM and 0.8 mM lactate, ratio=2;Figure 3A, Figure S2, Figure *S3*). Despite ample e-donor and e-acceptor available for growth, the high resource cultures entered a quasi-stationary phase at ~50 hours, after which there was continued slow growth (Figure 3A). Metabolite profiles showed that ammonium and N_2O production began simultaneously, as soon as nitrite was produced from nitrate reduction. The low resource cultures entered stationary phase at ~40 hours (Figure S2) after nitrate had been fully utilized. No further cell growth was observed after stationary phase was reached. These results show that cell growth occurred primarily on the reduction of nitrate, while nitrite reduction to ammonium and N_2O

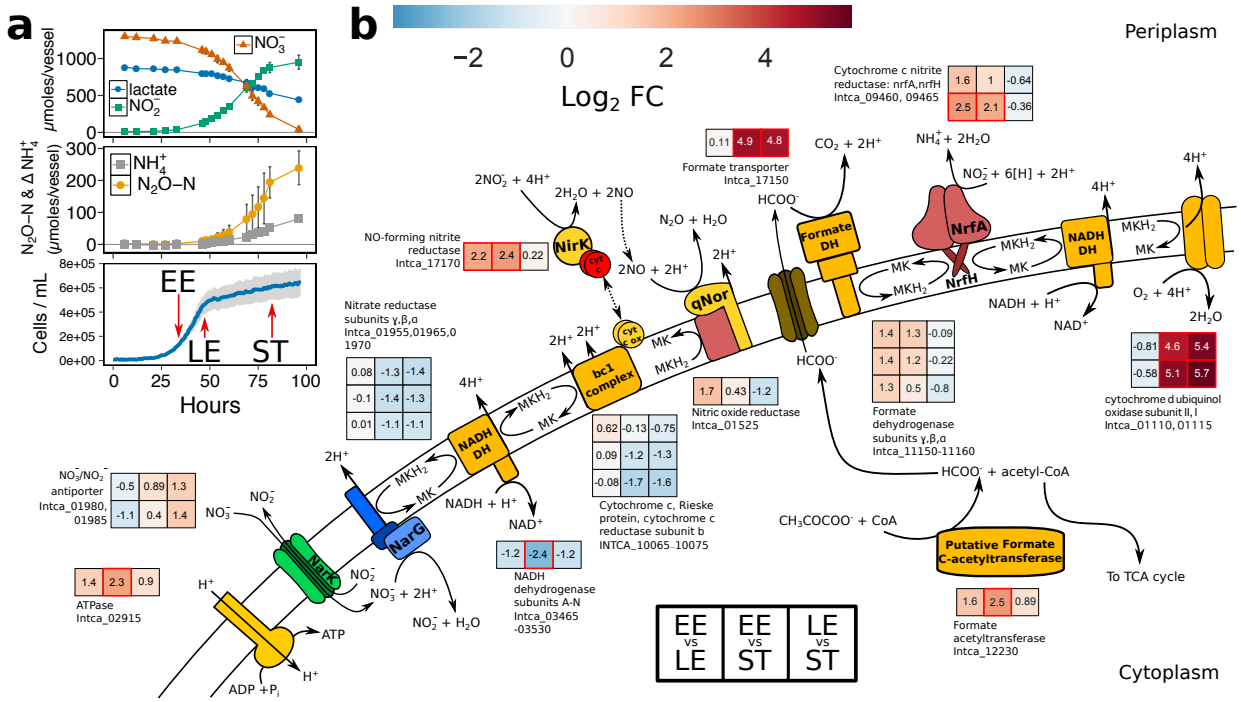

Figure 3. (A) Time-series metabolite profiles for lactate, nitrate, and nitrite (top pane), production of dissimilated end-products as N_2O-N and net change in NH_4^+ ammonium production (middle pane), and corresponding growth curve of *I. calvum* cells grown under 8mM lactate 12mM nitrate (C:NO_3^- ratio = 2) (bottom pane). Sampling points during growth phases are marked for transcriptomic analysis. (B) Metabolic reconstruction of the ETC from *I. calvum* with transcriptional changes for genes participating in dual-pathway dissimilatory nitrite reduction. Log_2 fold changes in transcript abundance are shown for late exponential relative to early exponential growth phase (EE vs. LE), stationary phase relative to early exponential growth phase (EE vs. ST), and stationary phase relative to late exponential growth phase (LE vs. ST). Locus IDs for each gene product correspond to heat map subplots in the order shown (left-to-right for each growth phase and top-to-bottom for each locus ID specified). Higher transcript abundance is represented in red, lower transcript abundance in blue, and no change in transcript abundance in white. Significant changes in transcript abundance ($p < 0.01$) are marked as a red box. Value of log_2 fold change is specified within each subplot. The log_2 fold changes of 14 NADH dehydrogenase subunits (Intca_03465-03530) were averaged as transcriptional changes were all shifted in the same direction.

occurred during a stationary growth phase, demonstrating that microbial activity is not always correlated with growth. The metabolite profiles for ammonium and N_2O at low resources (Figure S2) did not mirror those observed at high resources (Figure 3A). The rate of N_2O production significantly decreased and ammonium production oscillated rather than steadily increase through time. These differences in metabolite profiles, further demonstrate that concentration influences the activities of pathway bifurcation. Repeated time series experiments that were extended up to 300 hours show that nitrite is slowly depleted, but does not get fully consumed

206 (Figure *S3*). When cultures were given nitrite, instead of nitrate as a terminal electron acceptor (8
207 mM lactate, 12 mM nitrite; ratio=2), we observed no immediate growth (as was observed with
208 nitrate) but measured more N_2O than ammonium production (33.4±4.8 µmoles N_2O-N and
209 8.0±2.5 µmoles NH_4^+, respectively) (Figure S4), demonstrating respiratory ammonification does
210 not exceed denitrification when nitrite is supplied as the sole acceptor in *I. calvum*.

211 **Nitrite-reducing modules are up-regulated during late exponential- and stationary-phase**
212 **growth.** In order to gain insight into mechanisms of gene regulation and transcriptional
213 organization of *I. calvum*, we conducted RNA-Seq in parallel with the high resource time-series
214 metabolite profile (Figure 3A). This approach enabled us to compare genome-wide differential
215 expression based on $\log_2$ fold change (lfc) of RNA extracted from three growth phases: early
216 exponential (EE), late exponential (LE), and stationary (ST) (Figure 3B, Figure *S5*). Within the
217 central metabolic pathway beginning with the conversion of lactate to pyruvate, we observed a
218 moderate decrease in transcript abundance of L-lactate dehydrogenase (LDH) (Intca_16740)
219 between EE-LE and -ST (lfc = -1.6±0.7; -1.9±0.7), respectively. Lactate utilization protein C
220 (LUP) (Intca_04080), an enzyme involved in lactate degradation, also showed a moderate and
221 significant decrease in transcript abundance between EE-LE and -ST (lfc = -1.6±0.6; -2.4±0.6,
222 p=0.002), respectively. *I. calvum* encodes for two parallel metabolic pathways for pyruvate
223 conversion to acetyl-CoA: pyruvate dehydrogenase (PDH) (Intca_01255) and pyruvate
224 ferredoxin oxidoreductase (PFOR) (Intca_15510). For PDH, there was a significant and
225 moderate increase in transcript abundance between EE-LE and -ST (lfc = 2.1±0.6, p=0.002;
226 1.5±0.6), respectively. For PFOR, there was a minor decrease in transcript abundance between
227 EE-LE (lfc = -0.43±0.5), and then a moderate increase in transcript abundance between EE-ST
228 (1.1±0.5). Citrate synthase (Intca_04135), the enzyme catalyzing the conversion of acetyl-CoA
229 to citrate and the first step of the tricarboxylic acid (TCA) cycle, showed a highly significant
230 increase in transcript abundance between EE-LE and -ST (lfc = 4.3±0.5, p<0.001; 6.9±0.5,
231 p<0.001).

232 Within the ETC, there was moderate and significant decrease in transcript abundance for all
233 subunits from the primary dehydrogenase (*nuo* complex; Intca_03465-03539) between EE-LE
234 and -ST (lfc = -1.2±0.3; -2.4±0.6, p<0.001), respectively. Nitrate reductase subunits showed no
235 change in transcript abundance between EE-LE (lfc = 0.01±0.07) and moderately decreased in

236 abundance by ST (lfc = -1.2±0.1), which was corroborated by the depletion of nitrate during
237 stationary phase. There was a significant increase in transcript abundance of *nirK* (Intca_17170)
238 (lfc = 2.2±0.6, p=0.003; 2.4±0.6, p<0.001) and quinol dehydrogenase/membrane anchor subunit
239 *nrfH* (Intca_09465) (lfc = 2.5±0.6, p=0.001; 2.1±0.6, p=0.003) by EE-LT and EE-ST,
240 respectively, which coincided with nitrite production (Figure 3A). The catalytic subunit of the
241 cytochrome c nitrite reductase complex (*nrfA*) (Intca_09460) also increased moderately in
242 transcript abundance by EE-LT and EE-ST (lfc = 1.6±0.6; 1.0±0.6), respectively (Figure 3B).
243 Contrary to the transcript abundance patterns of *nirK* and *nrfAH*, nitric oxide reductase (qNor;
244 Intca_01525) transcripts moderately increased between EE-LT (lfc = 1.6±0.6) but decreased in
245 the successive time periods (lfc = 0.43±0.6 between EE-ST; lfc = -1.2±0.6 between LE-ST)
246 (Figure 3B).

247 There was a significant increase in transcript abundance of formate transporter *focA*
248 (Intca_17150) between EE-ST, as well as LE-ST (lfc = 4.9±0.7, p=0.002; 4.8±0.7, p=0.002;
249 respectively). We verified the production of formate in our ion chromatography measurements in
250 the range of 100-200μM following late exponential growth. We also observed a moderate
251 increase in transcript abundance of formate dehydrogenase (FDH) subunits (Intca_11150-
252 11160). These results implicate the activity of formate oxidation, which would contribute to a Δp
253 in the periplasm via a Q-loop mechanism and the reduction of MK for electron transfer to nitrite
254 via cytochrome c nitrite reductase. Considering that formate was not provided in our media
255 recipe, an alternative pathway for formate production must exist in *I. calvum*. We also observed
256 acetate production in similar concentrations as formate (100-200μM). In *E. coli*, formate is
257 produced anaerobically from the action of pyruvate formate lyase (PFL). We identified a putative
258 PFL based on genome annotation (Intca_12230), where transcript abundance also significantly
259 increased by ST. PFL is also highly sensitive to oxygen[27], which was also in agreement with a
260 significant increase in transcript abundance between EE-ST and LE-ST (Figure 3B) of
261 cytochrome *bd* oxidase (Intca_01110 and Intca_01115), which is thought to protect anaerobic
262 enzymes against oxidative stress[28].

263 **Discussion**

264 We challenge the paradigm that C:NO_3^- ratio controls pathway selection in a dual-pathway
265 organism based on a simple principle: ratios do not account for the abundance of growth-limiting

266 resources. We hypothesized that limitation in C or NO_3^- should better predict pathway selection
267 in a dual-pathway denitrifier/respiratory ammonifier. To test this hypothesis, we systematically
268 measured the response of the Gram-positive Actinobacterium *Intrasporangium calvum* C5 to the
269 same range of C:NO_3^- ratios at both high and low resource loadings to better resolve mechanisms
270 of pathway selection. We demonstrated that resource concentration, not C:NO_3^- ratio, influences
271 pathway selection. We found stronger support for respiratory ammonification preference under
272 C-limitation (at low C:NO_3^- ratios), which also grew at significantly higher growth rates (Figure
273 *2*). These results suggest that the NrfA complex, which receives electrons directly from the MK-
274 pool, is optimized to maximize power when one or more resources are limiting. These data,
275 together with metabolic reconstructions from metabolite and transcriptional profiles (Figure 3),
276 suggest that C:NO_3^- ratio alone is insufficient to explain pathway selection.

277 The theoretical basis for pathway selection is explained by the law of the minimum (LM) and the
278 maximum power principle (MPP), which state that growth is limited by the least abundant
279 resource and that biological systems are designed to maximize power in order to effectively
280 allocate energy to reproduction and survival[29,30], respectively. Here, it appears these two natural
281 theories are working together: when resources are limited, the cell utilizes the respiratory
282 pathway for growth that is optimized to maximize power. Power, in this case, is realized as
283 higher growth rates from the cultures exhibiting disproportionately higher ammonium production
284 than N_2O production (Figure *2*: high resources: C:NO_3^- ratio = 0.1; low resources: C:NO_3^- ratios
285 = 4, 1, 0.5, 0.1). More specifically, the bacterium must generate a greater Δp in order to
286 maximize power when starved for a growth limiting resource. This may help to further explain
287 how respiratory ammonification, which is overall energetically less favorable than denitrification
288 (lactate with nitrite: ΔG^o = -763.98 versus ΔG^o = -1196.93, respectively), can have higher growth
289 yields[31] and growth rates (Figure *2*, Figure S1) under C- and N-limitation due to the higher
290 energy yield on a per-nitrite basis (denitrification: -217 KJ per mole nitrite; respiratory
291 ammonification: -399 KJ per mole nitrite). For comparison, a total of 8 H^+ are translocated
292 during denitrification by *I. calvum* (not including nitrate reduction since both pathways share this
293 step) (Figure 3): NADH dehydrogenase translocates 4 H^+ per MKH_2 oxidized and the bc_1
294 complex translocates an additional 4 H^+ per MKH_2 oxidized. However, 2 H^+ must be consumed
295 in the periplasm to reduce nitrite to NO[32]. qNor has a net zero H^+ release (consumes 2 H^+ to
296 make N_2O but releases 2 H^+) without MKH_2 regeneration[33]. Thus, a net total of 6 H^+ are

297 translocated per nitrite reduced in denitrification with added biosynthetic costs of making the bc_1
298 complex and qNor. In respiratory ammonification, MK/MKH_2 redox pair is cycled between
299 NADH dehydrogenase and formate dehydrogenase. 6 electrons and 8 H^+ are needed to reduce
300 nitrite to ammonium, thus 3 MKH_2 are needed[16]. If MKH_2 is received from NADH
301 dehydrogenase, 12 H^+ are translocated plus 2 H^+ from FDH. As each MKH_2 is oxidized at the
302 binding site of NrfH, 2 H^+ are liberated[16], resulting in a net total of 12 H^+ translocated per nitrite
303 reduced for respiratory ammonification. This implies that the cell might deplete its NADH pool
304 more rapidly on a per nitrite basis. However, if more protons are pumped in the early stages of
305 growth, the cell would be allocating the ATP generated for anabolism, as evidenced by higher
306 growth rates in the cultures exhibiting higher amounts of respiratory ammonification (Figure *2*),
307 which is supported by the MPP.

308 Under our high resource conditions (Figure *2*; left panels), at $C:NO_3^-$ ratios ≥ 1, we observed that
309 denitrification prevailed and these cultures had lower growth rates than the predominantly
310 ammonium producing cultures. These high resource circumstances resulted in the production of
311 toxic intermediates (i.e., NO_2^- and possibly NO, albeit at undetectable levels), which may explain
312 why these cultures had lower growth rates (Figure *2*; left panels) and quasi-steady state growth
313 curves in our high resource metabolite profile (Figure 3A). Rowley and colleagues[34] reported
314 that at least 20% of the N_2O released during high C conditions were produced by competition
315 between nitrite and nitrate in the active-site of NarG. Under excess C concentrations, NarG
316 produces intracellular NO from NO_2^- and these intermediates are likely inhibitory to cell growth,
317 which may explain why our growth curves (Figure 3A) reached a quasi-steady state before
318 nitrate had been fully utilized (as compared to the low resource metabolite profile, Figure S2).
319 Furthermore, resources were not limiting growth under these conditions. Rather, the cells were
320 likely experiencing toxicity from NO and NO_2^- and thus the metabolic outcomes would be
321 beyond the scope of the LM and MPP. Nonetheless, these results clearly demonstrate that end-
322 product formation from the two resource concentrations tested, with the same $C:NO_3^-$ ratios, are
323 not identical thereby refuting the $C:NO_3^-$ control hypothesis.

324 We selected a single treatment (8 mM lactate, 12 mM nitrate; $C:NO_3^-$ ratio = 2), in which we
325 observed both denitrification and respiratory ammonification occurring simultaneously, for
326 RNA-Seq in order to gain insight into the transcriptional organization of actively growing *I.*

327 *calvum* cells (Figure 3). Strangely, we saw a decrease in transcript abundance encoding for two
328 enzymes known to convert lactate to pyruvate, LDH and LUP. While normalized read counts
329 (Figure *S5*) were generally consistent across growth phases, indicative of constitutive expression,
330 further research investigating the mode of anaerobic lactate oxidation in *I. calvum* would
331 illuminate how reducing equivalents are fed into its central metabolic pathway. For example, *S.*
332 *loihica* PV-4 is known to use lactate for both denitrification and respiratory ammonification, but
333 only uses acetate for denitrification[35]. Nonetheless, our transcriptomic data suggests that
334 pyruvate plays a central role in providing reducing equivalents to the TCA cycle as Acetyl-CoA,
335 as evidenced by significant upregulation in the genes encoding for pyruvate dehydrogenase and
336 citrate synthase, as well as apparent "leaking" via incomplete lactate oxidation through the
337 release of acetate and formate. Such leaking may be produced by a putative PFL, adding to the
338 diversity of C utilization pathways feeding the ETC, and thereby driving pathway selection for
339 nitrite reduction. Our transcriptomic results, coupled with a parallel metabolite profile (Figure 3),
340 also suggest that the dual-pathway is induced by the presence of nitrite, and is not constitutively
341 expressed like nitrate reductase, *narG*. Furthermore, it appears that the significant increase in
342 transcript abundance for the gene encoding the *bd* oxidase helps to protect the anaerobic-
343 dependent biochemical machinery against oxidative stress, thereby scavenging any residual
344 oxygen during anaerobic growth.

345 Our metabolite profiles for N oxyanion respiration and N_2O versus ammonium production show
346 conflicting patterns relative to previous studies (Figure 3A, Figure S2). Yoon and colleagues[36]
347 reported complete reduction of nitrate, production of nitrite, and then rapid consumption of
348 nitrite, with N_2O as the main end-product, by *S. loihica* PV-4 (5 mM lactate, 1 mM nitrate;
349 ratio=0.6). When Yoon and colleagues[36] replaced nitrate with nitrite as the dominant electron
350 acceptor (5 mM lactate, 1 mM nitrite, ratio=0.6), ammonification prevailed. Other research has
351 shown the same response to nitrite replacement and ammonification dominance using non-
352 fermentable C-sources (i.e., acetate) in chemostat enrichments of *Geobacter lovleyi*[37]. In our
353 work, nitrite was never fully depleted (Figure 3A, Figure S2, Figure *S3*) and when nitrite was
354 given as the only electron acceptor, the bacterium predominantly used denitrification but without
355 concurrent growth (Figure S4). Similar to our work, Kraft and colleagues[26] also reported
356 denitrification dominance when nitrite was supplied as the terminal acceptor. These differences

357 highlight an incomplete understanding for the molecular mechanisms underlying the framework
358 put forth by the LM and MPP.

359 A detailed look into the biochemistry of ETC complexes helps to shed light on the molecular
360 mechanisms modulating pathway bifurcation. For example, Yoon and colleagues[3] demonstrated
361 that elevated pH selects for ammonification in *S. loihica* PV-4. This phenotypic response is due
362 to a decrease in the midpoint potential of the Rieske protein at higher pH[38–40]. Thus, any
363 hindrance of electron flow through the bc_1 complex would ultimately reduce the activity of
364 downstream processes and promote alternative respiratory pathways. Nitrogen and C limitation
365 have also been shown to influence flux distributions in redox sensitive proteins, including those
366 found in electron transport[41]. A drop in the intracellular redox potential (redox poise) of the cell
367 due to resource limitation may decrease the midpoint potential of the Rieske protein and reduce
368 the activity of any downstream electron exit modules, such as NirK[42–44]. Thus, based on
369 fundamental principles of protein redox chemistry and thermodynamics, it becomes clear that
370 denitrification versus ammonification are likely not modulated by an arbitrary ratio of $C:NO_3^-$,
371 but rather by thermodynamic constraints of the Q-cycle[11,12]. The phenotypic response of higher
372 rates of denitrification over ammonification at high $C:NO_3^-$ ratios in other published studies[3,4]
373 may also be due to enrichment bias for organisms that utilize quinones with higher midpoint
374 potentials in their bioenergetic chains (Figure *1*). Bergdoll and colleagues[11] suggested that
375 comparisons of Rieske/cyt*b* complexes from organisms with high- and low-potential quinones
376 may help to reconcile the thermodynamic properties of Q-cycle function. However, most of our
377 understanding of denitrification bioenergetics is based on evolutionarily recent UQ-based HP
378 bioenergetic chains from Gram-negative *α*-, *β*-, *γ*-proteobacteria. Because *I. calvum* uses a MK-
379 based LP bioenergetic chain it may be possible that the differences in pathway selection across
380 treatments are unique to LP chains.

381 Piecing together the evolutionary history of the N-cycle using isotopic signatures for
382 geochemically available N module cofactors (i.e., Ni, Fe, and Mo) coupled to molecular
383 evolutionary analysis has revealed respiratory ammonification was likely a major component of
384 the Archean N-cycle[25]. Abiotic nitrite formation and depletion of ammonia through
385 photodissociation[45] would have created selective pressures for a dissimilatory N pathway that
386 also produced assimilatory N. We demonstrate that NrfA proteins are significantly enriched in N

387 compared to NirK (i.e., no evolutionary constraints to cost minimize N in the *nrfA* gene
388 product[15]) (Figure *1*B) and that ammonium production (without accumulation in the medium)
389 supports growth in *I. calvum* (Figure *1*C). The Nrf module is also relatively simplistic in that it
390 receives electrons directly from the quinol pool and not the bc_1 complex used in denitrification.
391 The early exit of electrons from the ETC (i.e., before reaching the bc_1 complex) suggests that Nrf
392 may have originated prior to the bc_1 complex. Furthermore, the quinol oxidation site (Q_o) of
393 cytochrome *b* contains a PDWY motif, indicative of an ancestral LP respiratory chain found in
394 many Gram-positive organisms[46]. However, there is still debate regarding the presence of a
395 cytochrome *bc* complex in the last universal common ancestor[46,47]. Lastly, the Nrf module is
396 wired to operate via a q-loop with formate dehydrogenase whose Mo-cofactors would have also
397 been bioavailable during the Archean, further supporting an early evolution.

398 In summary, we employ a new predictive framework that accounts for the biochemistry and
399 evolutionary history of N modules, ETC complexes, and pool quinones to suggest the
400 mechanisms by which these two pathways are regulated at the molecular level. With this
401 understanding, it may be possible to extend our framework to environmental microbial
402 populations and accelerate model development across different ecosystem scales (i.e., cross-scale
403 systems biology).

404 **Materials and Methods**

405 **Culture Conditions**

406 Sample collection: *I. calvum* was isolated from a groundwater well (GW247) collected on
407 2/18/2013 at Oak Ridge National Laboratory (Lat: 35.97990, Long: 84.27059) with a
408 groundwater temperature of 15.57 ºC, conductivity of 521.9 µS/cm, and pH of 7.71. *I. calvum*
409 was isolated and obtained from Dr. R. Chakraborty (Lawrence Berkeley National Laboratory).
410 We began our experimental process by first picking single colonies from LB agar plates and
411 transferring the clonal isolates to LB broth.

412 Media preparation: All subsequent cultures were grown at 30 ºC and shaken at 250 rpm. Nitrate
413 reducing minimal media was prepared with the following final concentrations: NaCl (0.6mM),
414 NH_4Cl (1.75mM) (for ammonium replete conditions but not used in NH4-deplete conditions),
415 MgCl2 (0.2mM), CaCl2 (0.04mM), KCl (0.1mM), K2HPO4 (0.01mM), NaHCO3- (0.3mM),

416 cysteine (1mM) as reducing agent, resazurin as redox indicator, and trace elements and trace
417 vitamin solutions as reported[35,48]. 1M sterile filtered (0.2µm) Concentrated stocks of 60% w/w
418 sodium DL-lactate solution (Sigma-Aldrich, St. Louis, MO, USA), sodium-nitrate and sodium-
419 nitrite (≥99%, Fisher Scientific, Pittsburg, PA, USA) were diluted into media prior to
420 autoclaving to achieve the desired $C:NO_3^-$ ratio. $C:NO_3^-$ ratio was calculated based on[3] where the
421 number of C atoms (n) in the e-donor is multiplied by the concentration of the e-donor, divided
422 by the number of N atoms in the e-acceptor multiplied by the concentration of the e-acceptor
423 (Table *S4*). Media preparation was conducted in a 2L Widdel Flask. After autoclaving, the media
424 was immediately put under an anoxic headspace (N2/CO2 80:20 mix) and sterile filtered
425 (0.2µm) trace elements, trace vitamins, and reducing agent were added. The media was cooled
426 under an anoxic headspace and buffered with bicarbonate to maintain a pH of 7.2. Hungate
427 technique was used to dispense media into culture tubes (20 mL) and serum vials (100 mL) pre-
428 flushed with a sterile stream of ultra-high purity (UHP) N_2 and sealed with blue 1" butyl rubber
429 stoppers. End-point cultures were grown in Balch tubes (18x150-mm glass tube) sealed with
430 butyl rubber stoppers. Cultures for time-course sampling were grown in 160ml serum vials. All
431 end-point experiments were terminated after 100 hours unless otherwise noted. Mean pH for all
432 culture vessels (time series and end-point; Table *S5*), measured at the end of each experiment,
433 was 7.3±0.05 (n=144)

434 **Analytical procedures**

435 <u>Growth Curve/Cell counts/Yield Measurements</u>: Growth curves were measured from scratch-
436 free Balch-tubes grown cultures using an automated optical density reader at OD_{600} nm
437 (Lumenautix LLC, Reno, NV). End-point cultures were monitored until all replicates reached
438 stationary phase (65-100 hours depending on $C:NO_3^-$ treatment) (Figure *S6*).

439 Cell counts were performed by fixing cells in 4% paraformaldehyde (final concentration) for 20
440 minutes, filtered onto 0.2µm pore-sized black polycarbonate filters, and washed three times with
441 phosphate buffered saline (PBS, pH 7.2). Filtered cells captured on the black polycarbonate
442 filters were stained with SYBR® Gold nucleic acid stain (10-minute incubation) (ThermoFisher
443 Scientific) and counted manually with a fluorescence microscope (Olympus BX60, Tokyo,
444 Japan). We collected cells from during lag phase, exponential phase, and stationary phase in
445 order to create a standard curve of cell counts versus optical density (OD_{600}). We fit a linear

446 model to cell count versus OD_{600} (R^2=0.99) and used the resulting linear equation for cell count
447 enumeration for growth curves during our various treatment conditions.

448 Biomass concentrations were measured by filtration and drying as per standard protocol[49] for
449 8mM lactate/12mM nitrate and 0.8mM lactate/1.2mM nitrate treatments and conducted in
450 parallel with growth curve/cell counts as described above. Analysis from triplicate cultures
451 yielded (0.064 ± 0.003) and (0.016 ± 0.001) mg of biomass (dry weight) ml^{-1} for 8mM and 0.8
452 mM lactate cultures, respectively. Cell counts from stationary phase cultures were (1.5 ± 0.05) x
453 10^7 and (1.16 ± 0.09) x 10^6 for 8mM and 0.8 mM lactate cultures, respectively. From these
454 values the dry weight of a single *I. calvum* cell was estimated to be 1.09 x 10^{-10} g. Growth yield
455 (*Y*) (Table S3) was calculated by dividing biomass (g) by lactate mass (g) and moles consumed,
456 as described by[50]. Lactate measurements are described below.

457 Ion and Gas Chromatography Measurements: A dual channel Dionex ICS-5000+ (Thermo
458 Scientific) was used to measure all anions (AS11-HC) and cations (CS-16) from the bacterial
459 growth media. New glass IC vials were used for every sample in order to ensure no cross
460 contamination of analytes. Headspace gas from Balch tubes and serum vials was sampled with
461 volume appropriate gastight syringes (Hamilton Company, Reno, NV) pre-flushed with UHP N_2.
462 For high and low nutrient treatments, 10µl and 100µl of headspace were sampled and diluted
463 into 12ml exetainters (Labco, Lampter, Wales, UK) over-pressurized with 15ml UHP N_2,
464 respectively. Similar dilutions were performed for nitrite as e-acceptor experiments, ammonium-
465 deplete experiments, and time-series experiments. For time-series experiments, an equal volume
466 of headspace gas that was removed at each time-point was replaced with sterile UHP N_2. N_2O
467 and NO were measured by gas chromatography (Shimadzu Greenhouse Gas Analyzer GC-2014)
468 using a 500µl injection volume. The rubber septa on the injection port of the GC was replaced
469 after 100 injections in order to prevent leakage of the sample after the injection needle was lifted
470 out from the injection port. Aqueous concentrations of N_2O were calculated using a Henry's
471 constant of 1.751 (mM (g)/mM (aq)) corrected for the medium's ionic strength and temperature.
472 A total of 8-11 replicates per treatment were analyzed for all experiments discussed in this work
473 (Table *S5*).

474 Ammonium production and thermodynamic calculations: All nitrogen needed for assimilation
475 must be first converted into ammonium[50]. This fact makes ammonium production measurements
476 via respiratory nitrite ammonification difficult since the cells simultaneous consume ammonium
477 for growth. Therefore, direct measurements of ammonium from IC or spectrophotometric
478 analyses would not yield accurate production values. Because *I. calvum* simultaneously
479 consumes ammonium as its sole N source for growth and produces ammonium via respiratory
480 nitrite ammonification, we first measured ammonium consumption with O_2 and lactate by
481 calculating the difference between starting and ending ammonium concentrations. These
482 ammonium consumption values were then normalized to lactate consumed (0.31µmols
483 NH_4^+/lactate) and to ammonium consumed per cell, which was calculated from average cell
484 number of stationary phase biomass (Figure *S6*) (7.07×10^{-7}µmols NH_4^+/cell). These two
485 ammonium consumption constants were used as two separate methods to compare ammonium
486 production based on actual starting and ending ammonium/lactate measurements and cell
487 number during nitrate reducing minimal media experiments.

488 For ammonium production normalized to lactate consumption, calculations are based on a mass
489 balance approach from[51] for Total Belowground Carbon Allocation (TBCA) but adapted for
490 nitrogen flux instead of carbon flux:

491 $$\text{Net } NH_4^+{}_{(APL)} = (\Delta\text{lactate}_{start\text{-}end} \times 0.31\mu\text{mols } NH_4^+/\text{lactate}) + \Delta NH_4^+{}_{end\text{-}start} \quad (1)$$

492 Here, the $\Delta\text{lactate}_{start\text{-}end}$ variable (µmols) is multiplied by the ammonium consumed per lactate
493 consumed constant (APL). This value is added to the $\Delta NH_4^+{}_{end\text{-}start}$ variable (µmols), denoted as
494 ending minus starting concentration, which defines whether the change in ammonium is positive
495 (more ammonium produced than consumed) or negative (more ammonium consumed than
496 produced). The ammonium production method using cell count (APC) is calculated as reported
497 by[35], where :

498 $$\text{Net } NH_4^+{}_{(APC)} = (\text{Cell Yield} \times 7.07\times10^{-7}\mu\text{mols } NH_4^+/\text{cell}) + \Delta NH_4^+{}_{end\text{-}start} \quad (2)$$

499 Where Cell Yield is the number of cells at stationary phase (Figure *S6*). Comparison of these two
500 ammonia production methods revealed that they are in agreement with each other for anaerobic
501 nitrate reducing media experiments (Figure *S7*). However, because the cell counts under low
502 nutrient treatments were at the lower limit of our standard curve (OD versus cell count), we

503 observed slightly more variability using the APC method. Lactate measurements by IC gave us
504 higher sensitivity over the large range of treatments tested, thus we report the APL method in the
505 main text as the most sensitive method for reporting ammonium production by respiratory
506 ammonification.

507 Thermodynamic calculations for anaerobic lactate oxidation with nitrate and nitrite were carried
508 out using standard Gibbs free-energy values defined by Thauer *et al*.,[52].

509 **Nucleic Acid Extraction and Sequencing**

510 DNA for genome sequencing was extracted with phenol-chloroform. The DNA quality and
511 integrity was verified on Agilent 2200 TapeStation and DNA was sequenced on the PacBio
512 platform (Duke Center for Genomic and Computational Biology).

513 For gene expression analysis, *I. calvum* cells were grown in 300 mL batch cultures under 8mM
514 and 0.8mM lactate (12mM and 1.2mM nitrate, respectively) (n=3). Growth curves were
515 monitored in real-time to collect cells during early-exponential, late-exponential, and stationary
516 phase. Upon sampling, culturing vessels were immediately incubated on ice, aseptically
517 transferred to 50 mL falcon tubes and immediately centrifuged at 15000 G for 5 minutes at 4 ºC.
518 Supernatant was immediately poured off and the cell pellets were harvested and stored in TRIzol
519 Reagent (Ambion RNA by Life Technologies) at -80 ºC until further processing. RNA was
520 extracted with TRIzol Reagent (Ambion RNA by Life Technologies), following the
521 manufacturer's protocol. The extraction was scaled up to 20 ml of TRIzol and performed in 50
522 ml conical tubes. RNA was resuspended in water, treated with Baseline-ZERO DNase
523 (Epicentre) and cleaned up with RNeasy MinElute Cleanup Kit (QIAGEN). Total extracted RNA
524 from each growth phase was quantified (RiboGreen RNA quantification), analyzed for RNA
525 integrity number (RIN) (RIN≥0.8 were used for sequencing), treated with RiboZero rRNA
526 removal kit (Illumina, San Diego, CA). Library preparation was performed with the TruSeq
527 Stranded mRNA Library Prep kit (Illumina, San Diego, CA) and sequenced using Illumina
528 NextSeq 500 2x150 Mid Output v2 platform, resulting in 10-15 million reads per sample.

529 **Phylogenetic, Genomic, and Transcriptomic Analysis**

530 Genomic DNA was assembled using Canu (version 1.7.1) with an estimated genome size of 5
531 million base pairs[53]. The resulting single contiguous fragment was aligned to the *I.* calvum 7KIP
532 genome (Acc: NC_014830.1) to compare sequence similarity in Mauve[54,55]. Genome annotation
533 for C5 was performed through the NCBI Prokaryotic Genome pipeline
534 (www.ncbi.nlm.nih.gov/genome/annotation_prok/). Additional gene prediction analysis and
535 functional annotation was performed by the DOE Joint Genome Institute (JGI) using the Isolate
536 Genome Gene Calling method (Prodigal V2.6.3 February, 2016) under the submission ID
537 172966. The complete genome sequence and annotation is available in the NCBI database under
538 the BioProject number PRJNA475609.

539 A set of 34 NrfA amino acid sequences, representing 33 complete genome sequences and 1
540 octaheme nitrite reductase (ONR) from known respiratory ammonification organisms were
541 downloaded from GenBank (Table *S1*). A multiple sequence alignment (MSA) was generated
542 from the sequences annotated as cytochrome c nitrite reductase and ONR using MUSCLE[56]. The
543 resulting alignment was visualized within MEGA5[57] where the alignment was manually screened
544 for the presence of conserved amino acid residues consistent with those found in NrfA (i.e.,
545 heme motifs). A maximum likelihood tree was created from the alignment using RAxML[58] with
546 500 bootstrap iterations. The presence of NapA, NarG, NirK, and Nor modules were manually
547 queried from each NCBI genome in our set and confirmed by MSA, as described above.
548 Metabolic pathway for pool quinone type was queried on BioCyc Pathway/Genome Database
549 (biocyc.org) for each organism in our set. The structure of *I. calvum*'s NirK protein was
550 predicted using the protein structure predicting algorithm Phyre2[59]. Protein atomic composition
551 for C and N was calculated from amino acid sequences as input files, as described by[14,15], using
552 custom python scripts for each element separately (github.com/dvuono/Cost_minimization).

553 For transcriptomic analysis, the resulting raw reads were inspected using FastQC[60] to determine
554 quality, read length, and ambiguous read percentage. Reads were trimmed based on quality score
555 with a sliding window of 5 base pairs, quality cutoff of 28, trailing cutoff quality score of 10, as
556 well as adapter contamination removal in Trimmomatic[61]. Due to the high similarity of C5 to
557 7KIP, reads were aligned to the *Intrasporangium calvum* genomic reference sequence and gtf file
558 (Acc: NC_014830.1) using the STAR RNA-seq aligner[62], with the --limitBAMsortRam
559 parameter set to the recommended value by STAR. Sequence reads were mapped to genomic

features to obtain count data using featureCounts[63]. Systematic changes across experimental conditions were performed on normalized read counts in DESeq2[64]. The RNA-seq data reported in this study are available within the NCBI BioProject number PRJNA475609.

Statistical analyses were conducted in the R environment for statistical computing (r-project.org). Data that was tested using parametric statistical analysis were first validated for normality by visualizing the data as a histogram and testing via Shapiro-Wilks test for normality.

ACKNOWLEDGMENTS. We thank F. von Netzer, K. Hunt, S Morales, N. Stopnisek, K. Meinhardt, W. Qin, N Elliot, T. Hazen, H. Carlson, B. Ramsey, A. Murray, Z. Harrold, T. Morgan, P. Longley, and R. Hallnan. This research was supported by a grant from the Nevada Governor's office of Economic Development (JG), by the Desert Research Institute (DRI) postdoctoral research fellowship program, and in part by Ecosystems and Networks Integrated with Genes and Molecular Assemblies (ENIGMA) (http://enigma.lbl.gov)—a Scientific Focus Area Program at Lawrence Berkeley National Laboratory under contract number DE-AC02-05CH11231 and funded in part by Oak Ridge National Laboratory under contract DE-AC05-00OR22725, and is based upon work supported by the U.S. Department of Energy, Office of Science, Office of Biological & Environmental Research.

References

1. Knowles, R. Denitrification. *Microbiol. Rev.* **46,** 43–70 (1982).

2. Tiedje, J. M., Sexstone, A. J., Myrold, D. D. & Robinson, J. A. Denitrification: ecological niches , competition and survival. *Antonie Van Leeuwenhoek* **48,** 569–583 (1982).

3. Yoon, S., Cruz-García, C., Sanford, R., Ritalahti, K. M. & Löffler, F. E. Denitrification versus respiratory ammonification: Environmental controls of two competing dissimilatory NO 3-/NO 2-reduction pathways in Shewanella loihica strain PV-4. *ISME J.* **9,** 1093–1104 (2015).

4. van den Berg, E. M., van Dongen, U., Abbas, B. & van Loosdrecht, M. C. Enrichment of DNRA bacteria in a continuous culture. *ISME J.* **9,** 2153–2161 (2015).

5. Schmidt, C. S., Richardson, D. J. & Baggs, E. M. Constraining the conditions conducive to dissimilatory nitrate reduction to ammonium in temperate arable soils. *Soil Biol. Biochem.* **43,** 1607–1611 (2011).

6. Hardison, A. K., Algar, C. K., Giblin, A. E. & Rich, J. J. Influence of organic carbon and nitrate loading on partitioning between dissimilatory nitrate reduction to ammonium (DNRA) and N2 production. *Geochim. Cosmochim. Acta* **164,** 146–160 (2015).

7. Fazzolari, É., Nicolardot, B. & Germon, J. C. Simultaneous effects of increasing levels of glucose and oxygen partial pressures on denitrification and dissimilatory nitrate reduction to ammonium in repacked soil cores. *Eur. J. Soil Biol.* **34,** 47–52 (1998).

8. Galloway, J. N. *et al.* The Nitrogen Cascade. *Bioscience* **53,** 341 (2003).

9. Moparthi, V. K. & Hägerhäll, C. The evolution of respiratory chain complex i from a smaller last common ancestor consisting of 11 protein subunits. *J. Mol. Evol.* **72,** 484–497 (2011).

10. Dibrova, D. V., Cherepanov, D. A., Galperin, M. Y., Skulachev, V. P. & Mulkidjanian, A. Y. Evolution of

595 cytochrome bc complexes: From membrane-anchored dehydrogenases of ancient bacteria to triggers of
596 apoptosis in vertebrates. *Biochim. Biophys. Acta - Bioenerg.* **1827,** 1407–1427 (2013).

597 11. Bergdoll, L., Ten Brink, F., Nitschke, W., Picot, D. & Baymann, F. From low- to high-potential bioenergetic
598 chains: Thermodynamic constraints of Q-cycle function. *Biochim. Biophys. Acta* **1857,** 1569–1579 (2016).

599 12. Schoepp-Cothenet, B. *et al.* Menaquinone as pool quinone in a purple bacterium. *Proc. Natl. Acad. Sci.* **106,**
600 8549–54 (2009).

601 13. Soo, R. M., Hemp, J., Parks, D. H., Fischer, W. W. & Hugenholtz, P. On the origins of oxygenic
602 photosynthesis and aerobic respiration in Cyanobacteria. *Science (80-.).* **355,** 1436–1440 (2017).

603 14. Baudouin-Cornu, P., Schuerer, K., Marlière, P. & Thomas, D. Intimate evolution of proteins: Proteome
604 atomic content correlates with genome base composition. *J. Biol. Chem.* **279,** 5421–5428 (2004).

605 15. Grzymski, J. J. & Dussaq, A. M. The significance of nitrogen cost minimization in proteomes of marine
606 microorganisms. *ISME J.* **6,** 71–80 (2012).

607 16. Einsle, O., Messerschmidt, A., Huber, R., Kroneck, P. M. H. & Neese, F. Mechanism of the six-electron
608 reduction of nitrite to ammonia by cytochrome c nitrite reductase. *J. Am. Chem. Soc.* **124,** 11737–11745
609 (2002).

610 17. Kraft, B., Strous, M. & Tegetmeyer, H. E. Microbial nitrate respiration - Genes, enzymes and environmental
611 distribution. *J. Biotechnol.* **155,** 104–117 (2011).

612 18. Godfrey, L. V. & Falkowski, P. G. The cycling and redox state of nitrogen in the Archaean ocean. *Nat.*
613 *Geosci.* **2,** 725–729 (2009).

614 19. Nitschke, W. & Dracheva, S. Reaction center associated cytochromes in Anoxygenic Photosynthetic
615 Bactera. in (eds. Blankenship, R., Madigan, M. & Bauer, C.) 775–805 (Kluwer Academic, 1995).

616 20. Lalucat, J., Bennasar, A., Bosch, R., Garcia-Valdes, E. & Palleroni, N. J. Biology of Pseudomonas stutzeri.
617 *Microbiol. Mol. Biol. Rev.* **70,** 510–547 (2006).

618 21. Suharti & de Vries, S. Membrane-bound denitrification in the Gram-positive bacterium Bacillus
619 azotoformans. *Biochem. Soc. Trans.* **33,** 130–133 (2005).

620 22. Heylen, K., Keltjens, J. & Stein, L. Y. Redundancy and modularity in membrane-associated dissimilatory
621 nitrate reduction in Bacillus. *Front. Microbiol.* **3,** 1–27 (2012).

622 23. Decleyre, H., Heylen, K., Bjorn, T. & Willems, A. Highly diverse nirK genes comprise two major clades
623 that harbour ammonium-producing denitrifiers. *BMC Genomics* **17,** 1–13 (2016).

624 24. Kalakoutskii, L. V., Kirillova, I. P. & Krassilnikov, N. A. a New Genus of the. *J. Gen. Microbiol.* **48,** 373-
625 79–85 (1967).

626 25. Klotz, M. G. & Stein, L. Y. Nitrifier genomics and evolution of the nitrogen cycle. *FEMS Microbiol. Lett.*
627 **278,** 146–156 (2008).

628 26. Kraft, B. *et al.* The environmental controls that govern the end product of bacterial nitrate respiration.
629 *Science (80-.).* **345,** 676–679 (2014).

630 27. Abbe, K. S., Takahashi, S. & Yamada, T. Invovlement of oxygen-sensitive pyruvate-formate lysase in
631 mixed-acid fermetnation by Streptococcus mutans under strictly anerobic conditions. *J. Bacteriol.* **152,** 175
632 (1982).

633 28. Das, A., Silaghi-Dumitrescu, R., Ljungdahl, L. G. & Kurtz, D. M. Cytochrome *bd* oxidase, oxidative stress,
634 and dioxygen tolerance of the strictly anaerobic bacterium *Moorella thermoacetica*. *J Bacteriol* **187,** 2020–

635 2029 (2005).

636 29. Lotka, A. J. Contribution to the Energetics of Evolution. *Proc. Natl. Acad. Sci.* **8,** 147–151 (1922).

637 30. DeLong, J. P. The maximum power principle predicts the outcomes of two-species competition experiments.
638 *Oikos* **117,** 1329–1336 (2008).

639 31. Strohm, T. O., Griffin, B., Zumft, W. G. & Schink, B. Growth yields in bacterial denitrification and nitrate
640 ammonification. *Appl. Environ. Microbiol.* **73,** 1420–1424 (2007).

641 32. Zumft, W. G. Cell biology and molecular basis of denitrification. *Microbiol. Mol. Biol. Rev.* **61,** 533–616
642 (1997).

643 33. Hemp, J. & Gennis, R. B. Diversity of the Heme-Copper Superfamily in Archaea: Insights from Genomics
644 and Structural Modeling. in *Results and Problems in Cell Differentiation* (eds. Schäfer, G. & Penefsky, H.
645 S.) 1–28 (Springer Science+Business Media, 2008).

646 34. Rowley, G. *et al.* Resolving the contributions of the membrane-bound and periplasmic nitrate reductase
647 systems to nitric oxide and nitrous oxide production in Salmonella enterica serovar Typhimurium. *Biochem.*
648 *J.* **762,** 755–762 (2012).

649 35. Yoon, S., Sanford, R. A. & Löffler, F. E. Shewanella spp. Use acetate as an electron donor for denitrification
650 but not ferric iron or fumarate reduction. *Appl. Environ. Microbiol.* **79,** 2818–2822 (2013).

651 36. Yoon, S., Sanford, R. A. & Löffler, F. E. Nitrite control over dissimilatory nitrate/nitrite reduction pathways
652 in Shewanella loihica strain PV-4. *Appl. Environ. Microbiol.* **81,** 3510–3517 (2015).

653 37. van den Berg, E. M., Rombouts, J. L., Kuenen, J. G., Kleerebezem, R. & van Loosdrecht, M. C. M. Role of
654 nitrite in the competition between denitrification and DNRA in a chemostat enrichment culture. *AMB*
655 *Express* **7,** 1–7 (2017).

656 38. Link, T. A., Hagen, W. R., Pierik, A. J., Assmann, C. & von Jagow, G. Determination of the redox
657 properties of the Rieske cluster of bovine heart bc1 complex by direct electrochemistry of a water- soluble
658 fragment. *Eur.J.Biochem.* **208,** 685–691 (1992).

659 39. Ugulava, N. B. & Crofts, A. R. CD-monitored redox titration of the Rieske Fe-S protein of Rhodobacter
660 sphaeroides: pH dependence of the midpoint potential in isolated bc1 complex and in membranes. *FEBS*
661 *Lett.* **440,** 409–413 (1998).

662 40. Zu, Y. *et al.* Reduction Potentials of Rieske Clusters: Importance of the Coupling between Oxidation State
663 and Histidine Protonation State. *Biochemistry* **42,** 12400–12408 (2003).

664 41. Ansong, C. *et al.* Protein redox dynamics during light-to-dark transitions in cyanobacteria and impacts due
665 to nutrient limitation. *Front. Microbiol.* **5,** 1–10 (2014).

666 42. Snyder, C. H., Merbitz-Zahradnik, T., Link, T. A. & Trumpower, B. L. Role of the Rieske Iron – Sulfur
667 Protein Midpoint Potential in the Protonmotive Q-Cycle Mechanism of the Cytochrome bc 1 Complex. *J.*
668 *Bioenerg. Biomembr.* **31,** 235–242 (1999).

669 43. Denke, E. *et al.* Alteration of the midpoint potential and catalytic activity of the Rieske iron-sulfur protein
670 by changes of amino acids forming hydrogen bonds to the iron-sulfur cluster. *J. Biol. Chem.* **273,** 9085–
671 9093 (1998).

672 44. Hunte, C., Solmaz, S., Palsdóttir, H. & Wenz, T. A structural perspective on mechanism and function of the
673 cytochrome bc1 complex. in *Results and Problems in Cell Differentiation* (eds. Schäfer, G. & Penefsky, H.
674 S.) 253–270 (Springer Science+Business Media, 2008).

675 45. Falkowski, P. G. Evolution of the nitrogen cycle and its influence on the biological sequestration of CO2 in

676 the ocean. *Nature* **387,** 272–275 (1997).

677 46. Kao, W. C. & Hunte, C. The molecular evolution of the Qo Motif. *Genome Biol. Evol.* **6,** 1894–1910 (2014).

678 47. Dibrova, D. V., Cherepanov, D. A., Galperin, M. Y., Skulachev, V. P. & Mulkidjanian, A. Y. Evolution of
679 cytochrome bc complexes: From membrane-anchored dehydrogenases of ancient bacteria to triggers of
680 apoptosis in vertebrates. *Biochim. Biophys. Acta - Bioenerg.* **1827,** 1407–1427 (2013).

681 48. Hillesland, K. L. *et al.* Erosion of functional independence early in the evolution of a microbial mutualism.
682 *Proc. Natl. Acad. Sci.* **111,** 14822–14827 (2014).

683 49. APHA. *Standard Methods for the Examination of Water and Wastewater*. (American Public Health
684 Association: Washington, DC, 2012). doi:ISBN 9780875532356

685 50. White, D. *The physiology and biochemistry of prokaryotes*. (Oxford University Press, 2000).

686 51. Giardina, C. P. & Ryan, M. G. Total belowground carbon allocation in a fast-growing Eucalyptus plantation
687 estimated using a carbon balance approach. *Ecosystems* **5,** 487–499 (2002).

688 52. Thauer, R. K., Jungermann, K. & Decker, K. Energy conservation in chemotrophic anaerobic bacteria.
689 *Bacteriol. Rev.* **41,** 100–180 (1977).

690 53. Koren, S. *et al.* Canu : scalable and accurate long- - - read assembly via adaptive k - - - mer weighting and
691 repeat separation. *Genome Res.* 1–35 (2017). doi:10.1101/gr.215087.116.Freely

692 54. Darling, A. C. E., Mau, B., Blattner, F. R. & Perna, N. T. Mauve : Multiple Alignment of Conserved
693 Genomic Sequence With Rearrangements. *Genome Res.* **14,** 1394–1403 (2004).

694 55. Darling, A. E., Mau, B. & Perna, N. T. Progressivemauve: Multiple genome alignment with gene gain, loss
695 and rearrangement. *PLoS One* **5,** e11147 (2010).

696 56. Edgar, R. C. MUSCLE: multiple sequence alignment with high accuracy and high throughput. *Nucleic Acids*
697 *Res.* **32,** 1792–7 (2004).

698 57. Tamura, K. *et al.* MEGA5: Molecular evolutionary genetics analysis using maximum likelihood,
699 evolutionary distance, and maximum parsimony methods. *Mol. Biol. Evol.* **28,** 2731–2739 (2011).

700 58. Stamatakis, A. RAxML version 8: A tool for phylogenetic analysis and post-analysis of large phylogenies.
701 *Bioinformatics* **30,** 1312–1313 (2014).

702 59. Kelley, L. A., Mezulis, S., Yates, C., Wass, M. & Sternberg, M. The Phyre2 web portal for protein
703 modelling, prediction, and analysis. *Nat. Protoc.* **10,** 845–858 (2015).

704 60. Andrews, S. FastQC: A quality control tool for high throughput sequence data. *Available online at: http://*
705 *www.bioinformatics.babraham.ac.uk/projects/fastqc.* (2010).

706 61. Bolger, A. M., Lohse, M. & Usadel, B. Trimmomatic: A flexible trimmer for Illumina sequence data.
707 *Bioinformatics* **30,** 2114–2120 (2014).

708 62. Dobin, A. *et al.* STAR: Ultrafast universal RNA-seq aligner. *Bioinformatics* **29,** 15–21 (2013).

709 63. Liao, Y., Smyth, G. K. & Shi, W. FeatureCounts: An efficient general purpose program for assigning
710 sequence reads to genomic features. *Bioinformatics* **30,** 923–930 (2014).

711 64. Love, M. I., Huber, W. & Anders, S. Moderated estimation of fold change and dispersion for RNA-seq data
712 with DESeq2. *Genome Biol.* **15,** 1–21 (2014).

713